Mon. Not. R. Astron. Soc. **279**, 1019–1025 (1996)

Dust emission from IRC+10216

Željko Ivezić and Moshe Elitzur
Department of Physics and Astronomy, University of Kentucky, Lexington, KY 40506-0055, USA
e-mail: ivezic@pa.uky.edu, moshe@pa.uky.edu

Accepted 1995 November 24. Received 1995 November 23; in original form 1995 July 31

ABSTRACT
Infrared emission from the dust shell around IRC+10216 is analysed in detail, employing a self-consistent model for radiatively driven winds around late-type stars that couples the equations of motion and radiative transfer in the dust. The resulting model provides agreement with the wealth of available data, including the spectral energy distribution in the range 0.5–1000 μm, and visibility and array observations. Previous conclusions about two dust shells, derived from modelling the data with a few single-temperature components of different radii, are not supported by our results. The extended, continuous temperature and density distributions derived from our model obviate the need for such discrete shells. The IR properties vary with the stellar phase, reflecting changes in both the dust condensation radius r_1 and the overall optical depth τ – as the luminosity increases from minimum to maximum, r_1 increases while τ decreases. We find that the angular size of the dust condensation zone varies from 0.3 arcsec at minimum light to 0.5 arcsec at maximum. The shortage of flux at short wavelengths encountered in previous studies is resolved by employing a grain size distribution that includes grains larger than $\sim$ 0.1 μm, required also for the visibility fits. This distribution is in agreement with the one recently proposed by Jura in a study that probed the outer regions of the envelope. Since our constraints on the size distribution mostly reflect the envelope's inner regions, the agreement of these independent studies is evidence against significant changes in grain sizes through effects like sputtering or grain growth after the initial formation at the dust condensation zone.

Key words: circumstellar matter – stars: individual: IRC+10216 – stars: late-type – stars: mass-loss – dust, extinction – infrared: stars.

1 INTRODUCTION

IRC+10216 (CW Leo, IRAS 09452+1330) is by far the brightest and best-studied mass-losing carbon star (Jura & Kleinmann 1989). Starting with Mitchell & Robinson (1980), several authors have performed radiative transfer calculations for the IR dust emission from this source. However, with the exception of Winters, Dominik & Sedlmayr (1994), all the previous studies were based on a prescribed r^{-2} radial density distribution that is not fully consistent with those of radiatively driven winds. Furthermore, although reasonable fits to the observed spectral energy distribution (SED) were generated over a wide range of wavelengths, none of the models produced enough flux shortward of 1–2 μm (e.g. Le Bertre 1987; Keady, Hall & Ridgway 1988; Griffin 1990; Lorenz-Martins & Lefèvre 1993). In addition, none of the models provides simultaneous agreement with spatially resolved observations at 2.2 μm (e.g. Martin & Rogers 1987).

The purpose of this work is to perform a self-consistent study that employs a dust density distribution determined from the solution of the coupled system of radiative transfer and hydrodynamics equations for the wind. The equations are described elsewhere (Netzer & Elitzur 1993; Ivezić & Elitzur 1995, hereafter IE95). As shown in IE95, the solution of this system is essentially determined by a single quantity – the flux-averaged optical depth τ_F. Once τ_F is determined, scaling relations listed in IE95 and in Ivezić & Elitzur (1996; hereafter IE96) can be used to constrain all other relevant quantities. In principle, the optical depth can be estimated from either the spectral shape $f_\lambda = F_\lambda/F$, where $F = \int F_\lambda d\lambda$ is the bolometric flux, or spatially resolved observations. However, since the latter depend also on the angular scale of the system, because of observational uncertainties the determination of optical depth from the spectral shape is much more reliable. In IE96 we describe a two-step modelling procedure, which we follow in this work. In the first step the dust characteristics and overall optical depth are constrained from the best fit to the spectral shape. Then, with the model prediction for the surface

brightness distribution based on these parameters, the spatially resolved observations are used in the second step to determine the angular size of the dust condensation zone.

The spectral energy distribution is discussed in Section 2, high-resolution observations in Section 3 and outflow dynamics in Section 4. The results are summarized and discussed in Section 5.

2 SPECTRAL ENERGY DISTRIBUTION

IRC+10216 is a long-period variable with a period of 638 d and a recent minimum at JD = 2447863 (Dyck et al. 1991). We limit our analysis to the periodical changes and do not consider the long-term modulations with time-scales of a few decades noted by Dyck et al. The surface brightness distribution at short wavelengths ($\lesssim$ 2–3 μm) is slightly asymmetric (e.g. Ridgway & Keady 1988; Kastner & Weintraub 1994). However, these spatial asymmetries decrease as the wavelength increases (e.g. de Batz 1988)* and our model assumes spherical symmetry. Slight disagreement between the model and observations can be expected at short wavelengths, a point further discussed in Section 5.

Our best-fitting model to the spectral shape is shown in Fig. 1 together with the observations. The thick solid line corresponds to maximum light, the thin solid line to minimum (where there are only five observational points). The inset compares the model results (solid line) with the *IRAS* LRS data. The model is primarily determined by the overall optical depth and the dust composition.† From previous work (e.g. Blanco et al. 1994), the dust grains around IRC+10216 are primarily composed of amorphous carbon with a minor inclusion of SiC to account for the 11.3-μm feature. With optical properties for amorphous carbon taken from Hanner (1988) and for SiC from Pégourié (1988), we find that the best fit to the 11.3-μm feature is obtained with a mixture of 95 per cent amorphous carbon and 5 per cent SiC (by mass), although varying the percentage of SiC in the range 3–8 per cent still produces satisfactory agreement. Griffin (1990) presents results for various SiC abundances. He obtains the best agreement for 17 per cent SiC, but the quality of his fit at 8 per cent is comparable. The slight difference between the conclusions of the two studies is insignificant and might be explained by the r^{-2} density law employed by Griffin instead of the hydrodynamic calculation done here. A broad emission feature between 24 and 30 μm (Forrest, Houck & McCarthy 1981) provides evidence for an additional component, probably MgS compound (Goebel & Moseley 1985). With the aid of spectroscopic data for MgS from Nuth et al. (1985) we estimate the abundance of this component to be less than 10 per cent, if this chemical identification is correct.

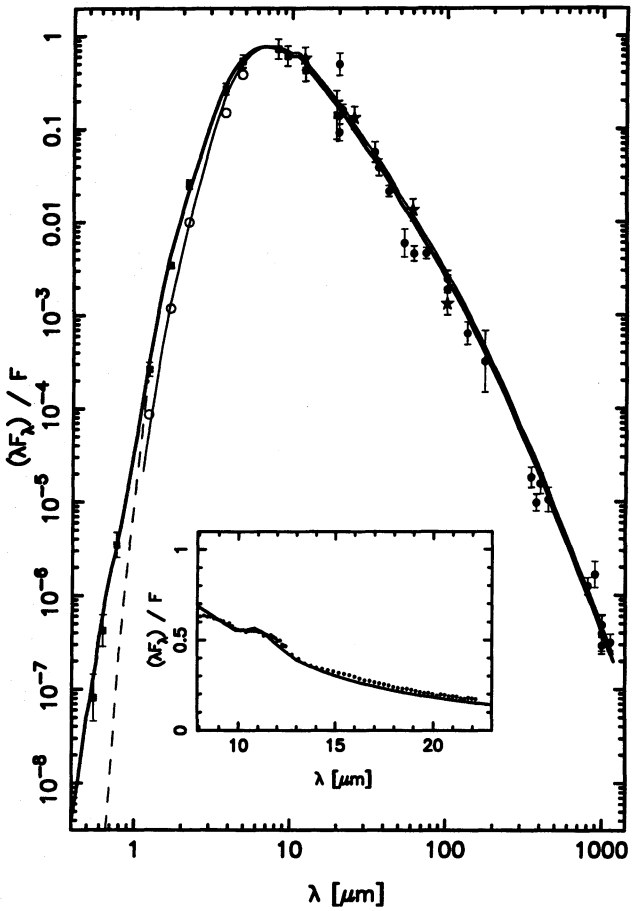

Figure 1. Spectral energy distribution for IRC+10216; lines represent model results, symbols the observations. Data are from Le Bertre (1987) (■), (1988) (○); Rengarajan et al. (1985) (●); and the *IRAS* Point Source Catalog (★). All observations are at maximum light except for those denoted by open circles, which are at minimum light. The thick solid line is the model result for maximum light, the thin solid line the result for minimum; details are described in the text. The dashed line is the model result for maximum light and single-size (0.05 μm) grains. The inset shows an expanded view of the *IRAS* LRS spectral region – the dots are the data, taken close to maximum light, the solid line the model.

In addition to the chemical composition, the distribution of grain radii a also affects the optical properties. However, the wavelength dependence of absorption and scattering efficiencies is independent of a once $\lambda \gtrsim 2\pi a$. Therefore, at the wavelengths of interest, $\lambda \geqslant 0.5$ μm, the grain size is irrelevant as long as $a \lesssim 0.1$ μm, and models of IRC+10216 usually assumed that all grains have the same size $a = 0.05$ μm (for an overview see Lorenz-Martins & Lefèvre 1993). The dashed line in Fig. 1 shows our model result for this single size, displaying the problems encountered by all other workers – the models do not produce enough flux at $\lambda \leqslant 1$ μm.

What is the meaning of this discrepancy? Dust emission is insignificant at $\lambda \lesssim 3$ μm because it decreases exponentially for wavelengths shorter than 3 μm × (1000 K/T_1), the peak wavelength of the Planck distribution for the dust condensation temperature T_1, the highest possible dust temperature. There-

* Recently, Sloan & Egan (1995) observed IRC+10216 with a 0.9×2.0 arcsec^2 resolution at 10 μm and obtained an indication of a blue emission patch with a size of ~ 1 arcsec, located ~ 1 arcsec north of the star. Note that these spatial details are comparable to the slit size; indeed, Sloan & Egan point out that this component's location could be an artefact of the reconstruction algorithm and that it could actually originate from the inner region centred on the star. Such emission indeed is expected from this region due to the hot dust. These observations do not seem to refute the findings of de Batz.

† The required grain properties are the spectral shapes of the absorption and scattering efficiencies. Absolute values of these quantities are not needed.

fore, the detected radiation involves only attenuated stellar emission and scattered light. Our detailed models show that, under these conditions, the spectral shape is proportional to $\exp(-\tau_{abs})$, where τ_{abs} is the overall optical depth for absorption. Therefore, the shortage of observed flux at $\lambda \lesssim 1$ μm implies that the model estimates for $\tau_{abs}(\lambda)$ at these wavelengths are too large. Since in general $\tau_{abs}(\lambda)$ increases as the wavelength decreases, this rise must be suppressed around 1 μm. Indeed, Rowan-Robinson & Harris (1983) noted that by postulating a departure from the usual λ^{-1} dependence of $\tau_{abs}(\lambda)$ to a flatter distribution at $\lambda \leqslant 1$ μm they could produce a better agreement with observations. Although they did not attempt to justify this behaviour, it can be modelled by assuming a range of grain sizes a. While $Q_{abs} \propto \lambda^{-1}$ for $\lambda \gtrsim 2\pi a$, it is approximately constant for $\lambda < 2\pi a$. Consequently, the flux shortage at $\lambda \lesssim 1$ μm can be alleviated by adding larger grains with sizes of $a \simeq \lambda/2\pi \approx 0.2$ μm, suppressing the rise of $\tau_{abs}(\lambda)$ when λ decreases below ~ 1 μm.

For the detailed models we employed two types of size distributions $n(a)$. Most often used is

$$n_{MRN}(a) \propto a^{-3.5}, \qquad a \leqslant a_{max} \tag{1}$$

proposed by Mathis, Rumpl & Nordsieck (1977). This MRN distribution includes a sharp cutoff, a_{max}, to the grain radii, required by the finite amount of mass in the dust. Recently Jura (1994) proposed a modification of the form

$$n_J(a) \propto a^{-3.5} e^{-a/a_0}, \tag{2}$$

replacing the sharp cutoff with an exponential one. Both distributions can produce satisfactory fits: the MRN distribution requires $a_{max} \approx 0.2$–0.3 μm, the Jura distribution $a_0 \approx 0.15$–0.2 μm. It appears that the Jura distribution produces a slightly better fit to the spectral shape observed at maximum light, but any stronger conclusion is hampered by the observational uncertainties. In contrast, recent models by Bagnulo, Doyle & Griffin (1995) produced satisfactory fits with single-size grains of 0.02 μm as well as the MRN distribution with $a_{max} = 0.05$ μm, but not with the Jura distribution. However, these models used an r^{-2} density law instead of employing a self-consistent hydrodynamic calculation, as done here. The two density distributions are substantially different at the inner regions – the self-consistent distribution has a much faster initial fall-off and has already dropped by a factor of 5 below the r^{-2} distribution at $r \sim 1.5 r_1$. Since this is the region where the short wavelengths are produced, this could account for the different results.

We have thus determined the two major ingredients that affect the spectral shape, the grain optical properties and overall optical depth. In addition, the stellar temperature T_* and dust condensation temperature T_1 have a discernible effect on the spectral shape, but only at short wavelengths. Our best fit gives $T_* = 2200 \pm 150$ K, an estimate in agreement with a spectral type of C9 (Cohen 1979) and the majority of other models. In general, the effect of T_* is limited to $\lambda \lesssim 4$ μm and its significance is diminished as the envelope's optical depth increases. Our best-fitting estimate for T_1 is 750 ± 50 K. The effect of T_1 is more significant because this parameter controls the peak wavelength of the spectral shape in envelopes that are optically thin around that peak. Our estimate for T_1, determined from the observed spectral shape by the location of the peak and the sharp decline toward short wavelengths, is somewhat lower than the ~ 1000 K obtained in most other models. Indeed, in these models the peak of the spectral shape is shifted slightly to the left, resulting in excessive flux in the 2–7 μm wavelength range (e.g., Le Bertre 1987; Lorenz-Martins & Lefèvre 1993).

Table 1. Overall optical depths for the best-fitting models plotted in Fig. 1. The last entry lists the flux-averaged optical depth τ_F. The other properties of the models are: dust composition, 95 per cent amorphous carbon and 5 per cent SiC (by mass); grain size distribution given in equation (2), with $a_0 = 0.2$ μm; dust condensation temperature $T_1 = 750$ K; stellar temperature $T_* = 2200$ K.

λ (μm)	$\varpi^{(a)}$	$\tau^{max(b)}$	$\tau^{min(c)}$
0.55	0.52	20	24
1.0	0.44	14	17
2.2	0.40	4.7	5.7
5.0	0.13	1.0	1.2
10	0.026	0.32	0.40
100	1.0×10^{-4}	0.01	0.012
—	—	2.0	2.4

(a) Albedo. (b) Total optical depth at maximum light. (c) Total optical depth at minimum light.

Finally, the radius of the envelope's outer edge, r_{out}, must be specified for a numerical solution. Because of scaling, only the relative thickness $y_{out} = r_{out}/r_1$ is needed. This parameter affects only the long-wavelength part of the solution, which is afflicted by a number of uncertainties. First, the behaviour of the absorption efficiency is quite uncertain at these wavelengths. Usually modelled by a power law $Q_{abs} \propto \lambda^{-\beta}$, the value of β is poorly known, typically taken as ~ 1–1.5. Next, the long-wavelength tail of the SED could contain a significant contribution from free–free emission (Griffin 1990). Fortunately, apart from the long-wavelength part of the SED, the model results are not very sensitive to these uncertainties. We find from fits to the spectral shape in the wavelength range 100–1000 μm that β varies from 1.2 to 1.6 for y_{out} between 600 and 10 000. An independent estimate for y_{out} can be obtained from the extent of molecular emission. CO observations by Huggins, Olofsson & Johansson (1988) indicate that $y_{out} \geqslant 700$, and consequently $\beta \geqslant 1.2$. Indeed, Jura (1983) suggested that $\beta = 1.3$, a proposal supported by Le Bertre (1987). The results presented in Fig. 1 are for $y_{out} = 700$ and $\beta = 1.3$. For this β, y_{out} can be increased all the way to 10 000 without a significant degradation of the fits.

The parameters of our best-fitting model are summarized in Table 1. Note again that the fit to the spectral shape f_λ is obtained without specifying the absolute size of the envelope, mass-loss rate, luminosity or distance to the star. For given dust grains, the resulting f_λ is primarily determined by the overall optical depth. Furthermore, the flux scale never entered the fitting procedure. Actual fluxes are obtained from f_λ through simple multiplication by the bolometric flux F. Comparison of fluxes from our best-fitting model with observations gives $F = 2.1 \times 10^{-8}$ W m^{-2} at maximum light, in agreement with Sopka et al. (1985). In IE96 we show that the bolometric flux and angular diameter of the dust condensation zone, $\theta_1 = 2r_1/D$ where D is the distance to the source, are related via

$$\theta_1 = 0.17\,\alpha \left(\frac{F}{10^{-8}\,\mathrm{W\,m^{-2}}}\right)^{0.5} \left(\frac{10^3\,\mathrm{K}}{T_1}\right)^2 \text{arcsec}, \tag{3}$$

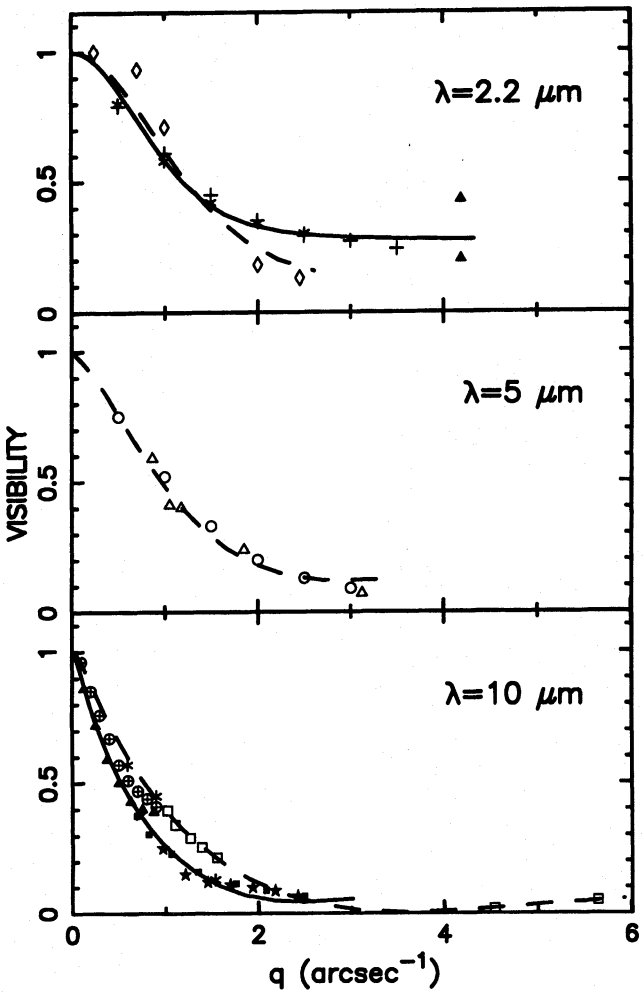

Figure 2. Visibility functions for IRC+10216. Lines represent model results, symbols the observations. Solid lines and full symbols (including + and *) correspond to phases close to maximum light, open symbols and dashed lines to phases close to minimum. Data are from Sutton, Betz & Storey (1979) (*), Selby, Wade & Sanchez Magro (1979) (◇), McCarthy, Howell & Low (1980) (△), Mariotti et al. (1983) (○), Dyck et al. (1984) (+), Dyck et al. (1987) (•), Benson, Turner & Dyck (1989) (⊕) and Danchi et al. (1990), (1994) (□). Phases and angular sizes of the dust condensation zone are listed in Table 2.

where α is a dimensionless coefficient of order unity characteristic of the model. This coefficient, determined theoretically from the overall solution, depends primarily on the grain optical properties and only slightly on T_*, T_1 and overall optical depth. From our best-fitting model for IRC+10216 we find that $\alpha = 1.3$ for this source, and therefore at maximum light $\theta_1^{\max} = 0.56$ arcsec. With an expected bolometric amplitude of 1 mag, $\theta_1^{\min} = 0.35$ arcsec at minimum light. These estimates for the angular scale must agree with high-resolution observations.

3 SPATIALLY RESOLVED OBSERVATIONS

In interpreting the spatially resolved observations of IRC+10216, the source variability must be taken into account. As the luminosity varies during the stellar cycle, the envelope temperature varies too. Therefore, as noted already by Danchi et al. (1990, 1994), the dust condensation radius varies during the stellar cycle and r_1 scales as $L^{0.5}$ (IE96). Because of the movement of the shell's inner boundary, the overall optical depth is expected to vary too, so that maximum light has minimum τ. With optical depths determined from the spectral shape we fit our models to visibility observations at minimum and maximum light obtained at 2.2, 5 and 10 μm. In these fits, θ_1 is taken as a free parameter, providing an independent estimate for it. Fig. 2 shows comparison of model results with observations. Since the data at 2.2 μm are spatially asymmetric, the plotted results are spatially averaged. Phases and values of θ_1 are summarized in Table 2. The independent fits for θ_1 from the visibility and the SED agree within 15–20 per cent on average. It can be estimated that, within 20 per cent, the angular size of the dust condensation point varies between 0.3 and 0.5 arcsec.

Table 2. Angular size of the dust condensation zone at maximum and minimum light determined from the available visibility observations. References for the observations are listed in the caption of Fig. 2.

λ (μm)	$\Phi^{(a)}$	$\theta_1{}^{(b)}$ (arcsec)	$\Delta^{(c)}$ (per cent)
2.2	max	0.40	29
2.2	min	0.29	17
5	min	0.32	8
10	max	0.45	20
10	min	0.30	14

(a) Phase of the light curve at which visibility observations were made at the wavelength listed in the first column.
(b) Angular size of the dust condensation zone determined from model fit to the visibility observations.
(c) The percentage difference between the angles listed in column (b) and those determined from equation (3) and the best fit to the SED (0.56 arcsec for max and 0.35 arcsec for min).

Previous models have never achieved simultaneous agreement for both the SED and spatially resolved observations at short wavelengths (e.g. Martin & Rogers 1987). In all these models, optical depths that fitted the SED produced a 2.2-μm visibility too large at $q \gtrsim 1$ arcsec^{-1}. This problem is directly related to the flux shortage of the models at these wavelengths and is another manifestation of the need for large grains. We have shown in IE96 that the value of the visibility when it levels off at large q is simply $\exp(-\tau_{\rm sca})$ for $\lambda \lesssim 3$ μm, where $\tau_{\rm sca}$ is the scattering optical depth. Therefore, $\tau_{\rm sca}$ must be increased to reduce the visibility. Also, because $\tau_{\rm abs}$ is fixed from the spectral shape, this increase translates to an increased albedo, implying the presence of grains with sizes of ~ 0.2 μm. This independent estimate of the grain sizes provides further support for the one obtained from the spectral shape.

Recently, Danchi et al. (1994) obtained visibility curves for IRC+10216 at 11 μm close to maximum and minimum light. From these observations they find $\theta_1 \approx 0.1$–0.2 arcsec, $\tau_{11} = 1.24$ and $T_1 = 1360$ K. These results, determined by fitting visibility curves at the single wavelength 11 μm, differ from ours; by comparison, from the spectral shape we find $\tau_{11} = 0.3 - 0.4$ and $T_1 = 750$ K. It is important to note that the Danchi et al. data, displayed as solid and open squares in the bottom panel of Fig. 2, are properly fitted by our models together with all other data. By contrast, the Danchi et al.

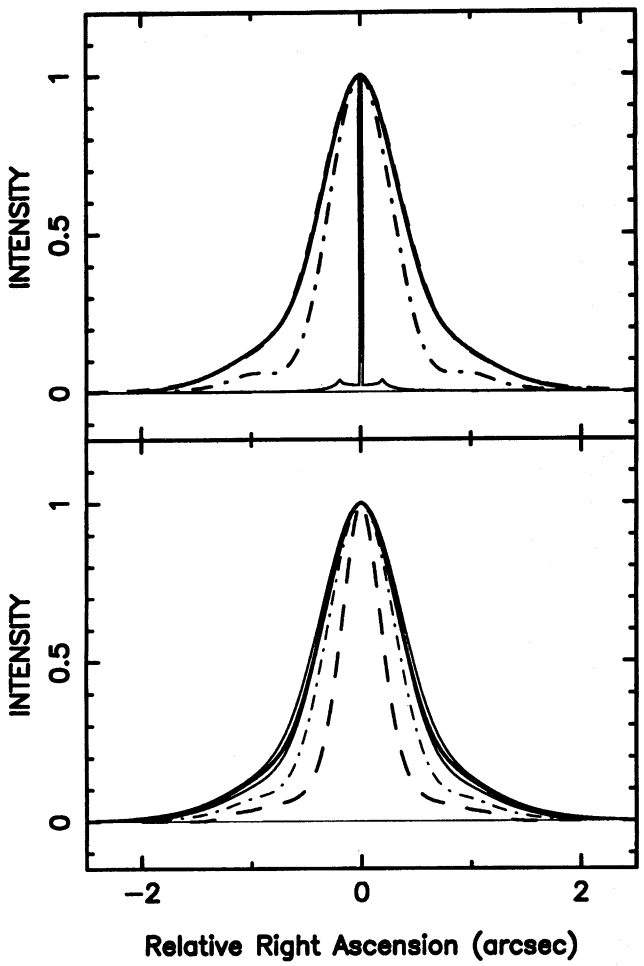

Figure 3. Single-scan (E–W) imaging of IRC+10216 at 10 μm. The thick solid line in the top panel is the observations of Bloemhof et al. (1988). Superimposed on it is our model result drawn as a dashed line, hardly distinguishable from the observations. It is obtained by a two-dimensional convolution of the surface brightness for $\theta_1 = 0.35$ arcsec (innermost thin solid line) with the point-spread function (PSF, dot-dashed line; all profiles are normalized to unity at the peak). In the bottom panel, the dashed line is the surface brightness deduced by Bloemhof et al. by one-dimensional deconvolution of the observed profile with the PSF. The dot-dashed line is the one-dimensional convolution of our model result with the PSF. The thick solid line is the two-dimensional convolution of our model result for $\theta_1 = 0.35$ arcsec with the PSF (the same as the dashed line in the top panel). The two thin solid lines below and above this curve correspond to curves derived analogously from models with $\theta_1 = 0.30$ and 0.40 arcsec, respectively.

fits rely on a limited data set, confined to a single wavelength and visibilities < 0.4, which does not sufficiently constrain the model parameters (IE96). Indeed, the values of τ_{11} and T_1 deduced by Danchi et al. cannot produce a simultaneous fit to the visibilities and SED at wavelengths shorter than 5–6 μm.

Bloemhof et al. (1988) obtained a single-scan image of IRC+10216 at 10 μm close to minimum light (phase $\simeq 0.4$). We computed the profile expected in those observations from the model surface brightness determined for this phase from the spectral shape. The top panel in Fig. 3 shows the comparison between the observed profile (outermost thick solid line) and our model result (dashed line, overlapping the observations; all displayed profiles are normalized to unity at their peaks).‡ The innermost thin solid line is the surface brightness distribution obtained from our model with $\theta_1 = 0.35$ arcsec. The central peak corresponds to the stellar contribution and the features at relative RA $\pm\theta_1/2$ to the dust formation zone. The model result is obtained from a two-dimensional convolution of this profile with the point-spread function (PSF), shown with the dot-dashed line. This fit to the observed image provides independent determination of θ_1 around minimum light, in agreement with the previous two.

Our model surface brightness is considerably different from the one deduced by Bloemhof et al., displayed with the dashed thick line in the bottom panel. In addition to the contribution of a central component with a width of ~ 0.4 arcsec, this profile also requires a more extended component with a width of ~ 2 arcsec. Bloemhof et al. obtained this distribution from a one- rather than a two-dimensional deconvolution of their observed profile with the PSF. We have verified that the results of the commonly used one-dimensional convolution with the PSF are indistinguishable from those of the proper two-dimensional convolution for centrally peaked surface brightness. However, in the case of extended structures whose peaks do not coincide with the centre of symmetry (e.g., a ring), the two procedures produce different results. A one-dimensional convolution of our model surface brightness with the PSF produces the thin dot-dashed line in the bottom panel, considerably different from the result of the proper two-dimensional convolution, repeated in the bottom panel as the thick solid line.

The possible existence of an extended $\sim$ 2-arcsec component was first conjectured from lunar occultation observations by Toombs et al. (1972) because they could not properly fit their results with a single, sharp-edged disc with a diameter of ~ 0.4 arcsec. Thus they invoked an additional, larger sharp-edged disc. Recently, Sloan & Egan (1995) also modelled their 10-μm observations, obtained with 0.9×2.0 arcsec^2 resolution, in terms of single-temperature components, a procedure that produced two dust shells. One shell ranges in diameter from 0.055 to 0.67 arcsec with a single temperature of 340 K, the other from 1.5 all the way to 5.2 arcsec with a single temperature of 240 K. However, our model, which has no sharp edges or discrete temperature components, properly explains both the Toombs et al. and Sloan & Egan observations because it is extended. Therefore, our modelling does not support the existence of the conjectured 2-arcsec component or any other discrete shell. We find no need to augment the steady-state outflow with any additional components.

Direct imaging is a most sensitive method for determining the dust condensation radius of optically thin envelopes. In the bottom panel of Fig. 3 we display in thin solid lines the imaging results expected with the PSF of Bloemhof et al. when θ_1 is varied by only $\pm$ 0.05 arcsec. Since the expected variation of θ_1 between minimum and maximum light is considerably larger, measurements of this variation during the stellar cycle can provide an important check of our models.

‡ To remove a slight asymmetry in the observations, all profiles are symmetrized east–west.

4 DYNAMICAL PROPERTIES

The quantities determined from IR observations can be used to constrain dynamical properties of the IRC+10216 outflow. Momentum flux conservation relates the mass-loss rate $\dot{M} = \dot{M}_{-5} \times 10^{-5}$ $M_\odot$ yr^{-1} and v_e, the terminal outflow velocity in km s^{-1}, to radiative properties via

$$\dot{M}_{-5} v_e = 20 \tau_F L_4 (1 - \Gamma^{-1}). \quad (4)$$

This relation is valid in steady-state for the time-averages of τ_F and the stellar luminosity $L_* = L_4 \times 10^4$ $L_\odot$, where Γ ($\propto M_*/L_4$) is the gravitational correction (IE95). Our model calculations give $\Gamma^{-1} = 0.13$ for IRC+10216 if the stellar mass is $M_* = 1$ $M_\odot$ and $L_4 = 1.5$; uncertainties in M_* and L_4 are of minor importance since Γ^{-1} is so small. From our models we find that τ_F varies from 2 at maximum light to 2.4 at minimum (see Table 1). With a terminal outflow velocity of 15 km s^{-1} (Morris, Lucas & Omont 1985; Zuckerman & Dyck 1986), this gives

$$\dot{M}_{-5} = 2.1 L_4, \quad (5)$$

where L_4 refers to the luminosity at maximum light, assuming a bolometric amplitude of 1 mag.

The dust mass-loss rate $\dot{M}^d$ is directly related to the optical depth via

$$\tau = \frac{3\dot{M}^d}{16\pi v_1 \rho_s r_1} \times \int_1^\infty \hat{n}_d(y)\,dy \int_0^\infty \frac{Q(a)}{a} n_J(a)\,da. \quad (6)$$

Here ρ_s is the dust solid density (1.85 g cm^{-3}, Rouleau & Martin 1991); $Q(a)$ is the extinction efficiency of grains with radius a; $\hat{n}_d$ is the dust density profile normalized to unity at r_1; and v_1 is the outflow velocity at r_1, assumed to be 1 km s^{-1}. This velocity corresponds to the velocity at the sonic point (Deguchi 1980) and introduces the principal uncertainty in determining $\dot{M}^d$. From this result and expressions for r_1 listed in IE96, our model calculations of IRC+10216 produce

$$\dot{M}^d_{-8} = 4.2\sqrt{L_4}, \quad (7)$$

where $\dot{M}^d_{-8} = \dot{M}^d/10^{-8}$ $M_\odot$ yr^{-1}; the variation with $\sqrt{L_4}$ reflects the dependence of r_1 on luminosity (cf. Section 3). The ratio of the mass-loss rates of the entire envelope and the dust component produces the average gas-to-dust ratio

$$r_{gd} = 1000 \frac{\dot{M}_{-5}}{\dot{M}^d_{-8}} = 500\sqrt{L_4}. \quad (8)$$

In all these relations, the luminosity remains unknown. Since the bolometric flux is 2.1×10^{-8} W m^{-2}, the luminosity obeys

$$L_4 = 1.5\, D^2_{150}, \quad (9)$$

where $D = D_{150} \times 150$ pc is the distance to the star. In terms of this parametrization, the various quantities listed above are

$$\dot{M}_{-5} = 3.1\, D^2_{150}, \quad \dot{M}^d_{-8} = 5.2\, D_{150}, \quad r_{gd} = 610\, D_{150}. \quad (10)$$

These results are in good agreement with independent estimates if we take $D = 150$ pc. Estimates for $\dot{M}_{-5}$ based on CO data range from 1–2 (Jura 1994, and references therein) to 4.7 (Kwan & Webster 1993). Values derived for $\dot{M}^d_{-8}$ vary from 5.6 (Griffin 1990) to 9.8 (Kastner 1992). Gas-to-dust ratios for carbonaceous winds in late-type stars range from 260 (Volk, Kwok & Langill 1992) to 670 (Knapp 1985).

The most-often quoted distance to IRC+10216 is 290 pc, derived by Herbig & Zappala (1970) for an assumed luminosity of $L_4 = 5.5$. This distance leads to unrealistically high mass-loss rates and gas-to-dust ratios. A closer distance of 100–150 pc has been proposed by Zuckerman, Dyck & Claussen (1986) and Kastner (1992), and our results support these suggestions. Based on theoretical considerations, Martin & Rogers (1987) pointed out that $L_4 \geqslant 1.2$. Thus, IRC+10216 is probably not closer than 130 pc, and the value of 150 pc adopted by Jura (1994) and in this work is likely to be close to the true distance. With this distance of 150 pc, the radius of the dust condensation zone varies from $\sim 3 \times 10^{14}$ cm at minimum light to $\sim 5 \times 10^{14}$ cm at maximum.

5 DISCUSSION

Our model for IRC+10216 provides a description of the IR observations based on a self-consistent treatment of the dynamics and radiative transfer. The model provides simultaneous agreement for both the SED and all high-resolution observations of this star. Particularly encouraging is the agreement between the three independent determinations of the angular size of the dust condensation point ($\sim$ 0.3 arcsec at minimum light). Our results demonstrate the advantage of following the two-step modelling procedure outlined in the Introduction. The most appropriate approach is first to constrain the overall optical depth by the spectral shape, then use visibility data to determine the size of the envelope.

Because of the close agreement obtained for such a variety of independent observations, we do not expect major changes in the parameters determined here. The model could still be improved by considering the asymmetry of the envelope. As mentioned in Section 2, although symmetric at wavelengths longer than $\sim$ 3–4 μm, the observed surface brightness is slightly asymmetric at short wavelengths. Such a dual appearance can be understood in terms of the basic physical processes that control the IR radiation at the different spectral regions. At short wavelengths, scattering dominates the observed radiation. Since scattering can be expected to map the entire envelope, scattered radiation should reflect the density distribution, displaying any asymmetry in it. As long as the elongation is not severe, it is reflected only in the shape of the image, not in the flux. On the other hand, radiation at longer wavelengths is dominated by dust emission, predominantly controlled by the dust temperature distribution. For slightly elongated density distributions, the dust temperature distribution can still be spherically symmetric to a good degree of approximation because it is mostly controlled by the distance from the central star. This explains the close agreement of our spherically symmetric model with the data. A slightly enhanced mass-loss rate in the equatorial plane, as proposed by Ridgway & Keady (1988) and supported by Kastner & Weintraub (1994), can be accommodated without a significant effect on our results. On the other hand, our model cannot describe the emission from a bipolar nebula, the geometry suggested for IRC+10216 by Dyck et al. (1987), and its success indicates that such a drastic departure from spherical symmetry may not be necessary to explain the observations.

We resolve the difficulties encountered in previous stud-

ies at short wavelengths by including large grains. The short-wavelength behaviour of both the SED and the visibility shows that grains as large as $\sim$ 0.15–0.2 μm are present. Jura (1994) recently discussed the grain size distribution for IRC+10216, based on polarization in the *K* band and shielding of circumstellar molecules against destruction by interstellar UV radiation. He finds that grains as large as $\sim$ 0.1 μm exist in the outer envelope (more than 15 arcsec from the star), in good agreement with the sizes obtained here. Since our analysis of grain sizes is primarily affected by the inner regions of the envelope while Jura's results apply to the outer regions, we conclude that the grain sizes do not change significantly through the envelope. The effects of sputtering, grain growth, etc., do not seem to be too important after the initial dust formation.

ACKNOWLEDGMENTS

We thank E. Bloemhof and R. Danen for providing us with observations of IRC+10216. We are especially indebted to E. Bloemhof for his generous help in clarifying the analysis of the data. We also thank the referee, C. Skinner, for his careful reading and useful comments. This research has made use of the SIMBAD database, operated at CDS, Strasbourg, France, and the ADS database. Support by NSF grant AST-9321847, NASA grant NAG 5-3010 and the Center for Computational Sciences of the University of Kentucky is gratefully acknowledged.

REFERENCES

Bagnulo S., Doyle J.G., Griffin I.P., 1995, A&A, 301, 501
Benson J.A., Turner N.H., Dyck H.M., 1989, AJ, 97(6), 1763
Blanco A., Borghesi A., Fonti S., Orofino V., 1994, A&A, 283, 561
Bloemhof E.E., Danchi W.C., Townes C.H., McLaren R.A., 1988, ApJ, 333, 300
Cohen M., 1979, MNRAS, 186, 837
Danchi W.C., Bester M., Degiacomi C.G., McCullough P.R., Townes C.H., 1990, ApJ, 359, L59
Danchi W.C., Bester M., Degiacomi C.G., Greenhill L.J., Townes C.H., 1994, AJ, 107(4), 1469
de Batz B., 1988, A&AS, 76, 5
Deguchi S., 1980, ApJ, 236, 567
Dyck H.M., Zuckerman B., Leinert Ch., Beckwith S., 1984, ApJ, 287, 801
Dyck H.M., Zuckerman B., Howell R.R., Beckwith S., 1987, PASP, 99, 99
Dyck H.M., Benson J.A., Howell R.R., Joyce R.R., Leinert Ch., 1991, AJ, 102(1), 200
Forrest W.J., Houck J.R., McCarthy J.F., 1981, ApJ, 248, 195
Goebel J.H., Moseley S.H., 1985, ApJ, 290, L35
Griffin I.P., 1990, MNRAS, 247, 591
Hanner M.S., 1988, Infrared Observations of Comets Halley and Wilson and Properties of the Grains. NASA89-13330, p. 22
Herbig G.H., Zappala R.R., 1970, ApJ, 162, L15
Huggins P.J., Olofsson H., Johansson L.E.B., 1988, ApJ, 332, 1009
Ivezić Ž., Elitzur M., 1995, ApJ, 445, 415 (IE95)
Ivezić Ž., Elitzur M., 1996, MNRAS, 279, 1011 (IE96, this issue)
Jura M., 1983, ApJ, 267, 647
Jura M., 1994, ApJ, 434, 713
Jura M., Kleinmann S.G., 1989, ApJ, 341, 359
Kastner J.H., 1992, ApJ, 401, 337
Kastner J.H., Weintraub D.A., 1994, ApJ, 434, 719
Keady J.J., Hall D.N.B., Ridgway S.T., 1988, ApJ, 326, 832
Knapp G.R., 1985, ApJ, 293, 273
Kwan J., Webster Z., 1993, ApJ, 419, 674
Le Bertre T., 1987, A&A, 176, 107
Le Bertre T., 1988, A&A, 203, 85
Lorenz-Martins S., Lefévre J., 1993, A&A, 280, 567
Mariotti M., Chelli A., Foy R., Léna P., Sibille F., Tchountov G., 1983, A&A, 120, 237
Martin P.G., Rogers C., 1987, ApJ, 322, 374
Mathis J.S., Rumpl W., Nordsieck K.H., 1977, ApJ, 217, 425
McCarthy D.W., Howell R., Low F.J., 1980, ApJ, 235, L27
Mitchell R.M., Robinson G., 1980, MNRAS, 190, 669
Morris M., Lucas R., Omont A., 1985, A&A, 142, 107
Netzer N., Elitzur M., 1993, ApJ, 410, 701
Nuth J.A., Moseley S.H., Silverberg R.F., Goebel J.H., Moore W.J., 1985, ApJ, 290, L41
Pégourié B., 1988, A&A, 194, 335
Rengarajan T.N., Fazio G.G., Maxson C.W., McBreen B., Serio S., Sciortino S., 1985, ApJ, 289, 630
Ridgway S.T., Keady J.J., 1988, ApJ, 326, 843
Rouleau F., Martin P.G., 1991, ApJ, 377, 526
Rowan-Robinson M., Harris S., 1983, MNRAS, 202, 797
Selby M.J., Wade R., Sanchez Magro C., 1979, MNRAS, 187, 553
Sloan G.C., Egan M.P., 1995, ApJ, 444, 452
Sopka R.J., Hildebrand R., Jaffe D.T., Gatley I., Roellig T., Werner M., Jura M., Zuckerman B., 1985, ApJ, 294, 242
Sutton E.C., Betz A.L., Storey J.W.V., 1979, ApJ, 230, L105
Toombs R.I., Becklin E.E., Frogel J.A., Law S.K., Porter F.C., Westphal J.A., 1972, ApJ, 173, L71
Volk K., Kwok S., Langill P.P., 1992, ApJ, 391, 285
Winters J.M., Dominik C., Sedlmayr E., 1994, A&A, 288, 255
Zuckerman B., Dyck H.M., 1986, ApJ, 304, 394
Zuckerman B., Dyck H.M., Claussen M.J., 1986, ApJ, 304, 401

This paper has been produced using the Royal Astronomical Society/Blackwell Science LaTeX style file.